Dendritic NMDA receptors in parvalbumin neurons enable strong and stable neuronal assemblies

Jonathan Cornford[1], Marion S Mercier[1]†, Marco Leite[1]†, Vincent Magloire[1], Michael Häusser[2], Dimitri M Kullmann[1*]

Affiliations:

[1]Institute of Neurology, University College London,

[2]Wolfson Institute for Biomedical Research, University College London,

*Correspondence to: d.kullmann@ucl.ac.uk

†These authors contributed equally

Abstract: Deletion of NMDA receptors from parvalbumin-positive (PV+) interneurons disrupts gamma oscillations and destabilizes hippocampal spatial representations. How do NMDA receptors contribute to synaptic integration by PV+ interneurons to support robust neuronal assemblies? We show, using two-photon glutamate uncaging, that NMDA receptors underlie supralinear summation of synaptic inputs in mouse hippocampal CA1 PV+ interneurons, but only in dendrites innervated by feedback connections from local pyramidal neurons. Incorporating NMDA receptors at feedback connections in an oscillating excitatory-inhibitory spiking neural network provided for cooperative interactions among clustered inputs, and increased the stability of cell assemblies in the face of distracting inputs. Disrupted cell assembly interactions may underlie cognitive and sensory gating deficits seen with impaired NMDA receptor signaling in PV+ interneurons.

One Sentence Summary: Supralinear dendritic integration via NMDA receptors provides a mechanism for input gating in gamma-oscillating circuits.

Main Text

The formation and interaction of cell assemblies are central to information representation and processing[1]. Recruitment of local PV+ interneurons, which contribute to gamma band (30-100 Hz) oscillations and feedback inhibition of pyramidal neurons, is a strong candidate mechanism to mediate selection among competing cell assemblies[2–4]. Fast-spiking PV+ interneurons are innervated by both local feedback and extrinsic feedforward afferents, but how these sources of excitation interact is incompletely understood. PV+ interneurons, of which basket cells are the largest subset, have biophysical properties suited to rapid recruitment and fast inhibition of target neurons[5]. These features are critical to feedforward functions such as enforcement of narrow temporal integration and input normalization in principal neurons[6,7]. PV+ interneurons are also equipped with NMDA receptors (NMDARs), although these receptors contribute relatively less to synaptic excitation than in principal neurons. The slow kinetics and nonlinear voltage dependence of NMDARs do not appear well suited to fast signaling. Nevertheless, impaired NMDAR-mediated signaling in PV+ interneurons has been implicated in a range of network disorders including gamma rhythm disruption[8], impaired spatial representations[9], and human pathologies including schizophrenia[10]. Consistent with a role in cell assembly selection and stabilization, NMDARs have been reported to contribute to synaptic excitation of hippocampal PV+ interneurons predominantly at feedback connections from local pyramidal neurons[11]. In principal neurons, NMDAR-mediated dendritic nonlinearities greatly enhance the computing capacity of individual cells[12–15]. We therefore hypothesized an analogous function for NMDARs on PV+ interneurons.

To establish if NMDARs mediate integrative dendritic nonlinearities, akin to those seen in pyramidal neurons, we recorded somatic responses to two-photon glutamate uncaging at multiple dendritic sites of fast-spiking PV+ interneurons in hippocampal CA1 (**Fig. 1A**). Activation of individual uncaging locations produced glutamate-uncaging evoked excitatory postsynaptic potentials (uEPSPs) that were comparable to spontaneous EPSPs (**Fig. 1B** and Fig. S1), consistent with a high density of excitatory synapses reported in PV+ interneuron dendrites[16]. To assess nonlinear dendritic integration, we compared compound uEPSPs elicited by near-synchronous activation

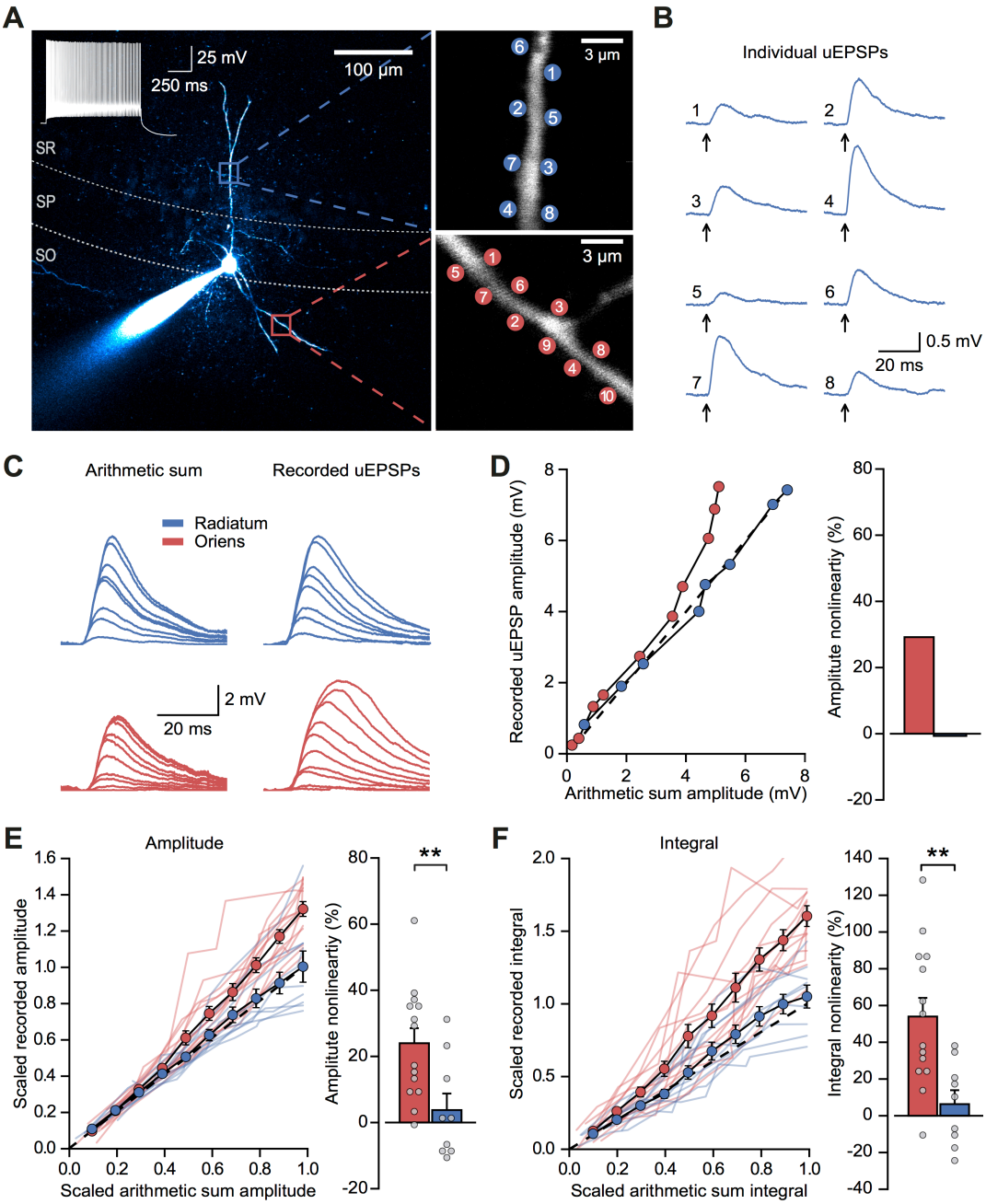

Figure 1: Differential input integration at stratum oriens and stratum radiatum dendrites of PV+ interneurons. (**A**) Two-photon z-projection image of a PV+ interneuron recorded via a patch pipette in stratum pyramidale (SP) and filled with Alexa-594 (left), with two dendritic regions of interest at higher magnification (right: top, stratum radiatum, SR; bottom, stratum oriens, SO), showing glutamate uncaging locations (numbered). (**B**) Individual uEPSP responses from radiatum dendritic locations shown in **A**. (**C**) Comparison of arithmetic sum of individual uEPSPs and recorded uEPSPs evoked by near-synchronous uncaging at multiple locations in stratum radiatum (blue) and oriens (red). (**D**) Peak amplitudes of recorded uEPSPs plotted against arithmetically summed waveforms for the two regions shown in **A**. Dashed line shows line of identity. Right: bar chart showing percentage amplitude nonlinearity. Red: oriens, blue: radiatum. (**E**) Summary of scaled peak amplitude comparisons for all cells (oriens locations: n = 14, radiatum locations: n = 9). Filled circles and error bars indicate mean ± SEM. Right: bar chart showing quantification of amplitude nonlinearity. (**F**) Time-integral nonlinearity plotted as for (E). **: $p < 0.01$.

of increasing numbers of uncaging locations to the arithmetic sum of individual responses (**Fig. 1C**). Activation of sites on dendrites in stratum oriens, which are innervated by local pyramidal neurons, revealed supralinear uEPSP summation (peak amplitude nonlinearity: 24.0 ± 4.5%, mean ± SEM, n = 14; **Fig. 1D, E**; unscaled responses in Fig. S2). This nonlinearity was even larger when measured using the time-integral of uEPSPs (time-integral nonlinearity from 0 to 50 ms: 54.0 ± 10.1%; **Fig. 1F**).

In contrast, when glutamate was uncaged along dendritic segments in stratum radiatum, which are innervated by Schaffer collaterals of CA3 pyramidal neurons but not by feedback axons, uEPSPs summated in a linear fashion (peak amplitude nonlinearity: 3.8 ± 5.0%, time-integral nonlinearity: 6.3 ± 7.6%, n = 9; oriens vs. radiatum $P = 0.0083$ and $P = 0.0028$ for peak amplitude and time-integral comparisons respectively, unpaired *t*-test, **Fig. 1D–F**). The difference between strata was also observed in the subset of paired cell-wise recordings (Fig. S3) and in simulations incorporating polyamine modulation of AMPA receptors (Fig. S4). Dendrites of PV+ interneurons mediating feedback inhibition, but not feedforward inhibition, thus exhibit supralinear input integration. We observed no significant relationships between integration nonlinearity and either distance from soma or the size of the arithmetic sum of the uEPSPs (Fig. S5).

Supralinear dendritic summation in stratum oriens was abolished when NMDARs were blocked with D(−)-2-Amino-5-phosphonopentanoic acid (D-AP5, 100 μM) (time-integral nonlinearity: 2.5 ± 3.0 %, vs control $P = 0.0004$, n = 10; **Fig. 2A–C**). Dendritic integration in stratum radiatum was unchanged from control conditions (time-integral nonlinearity: 3.3 ± 2.6 %, vs control $P = 0.88$, n = 4; **Fig. 2A–C**). In contrast to D-AP5, the sodium channel blocker tetrodotoxin (TTX, 100 nM) did not significantly affect integration in either stratum oriens or radiatum (oriens time-integral nonlinearity 40.1 ± 5.6 %, vs control $P = 0.23$, n = 16; radiatum time-integral nonlinearity 9.4 ± 3.3 %, vs control $P = 0.71$, n = 9; **Fig. 2D**). Similar results were obtained when measuring peak uEPSP amplitudes instead of time-integrals (Fig. S6). Distances from soma and somatic uEPSP amplitudes were comparable across all conditions (Fig. S7). NMDARs are thus necessary for supralinear dendritic

integration in the feedback circuit. Furthermore, failure of TTX to affect uEPSP integration in dendrites in either stratum is consistent with the view that dendrites do not support regenerative events[17] (although see [18]).

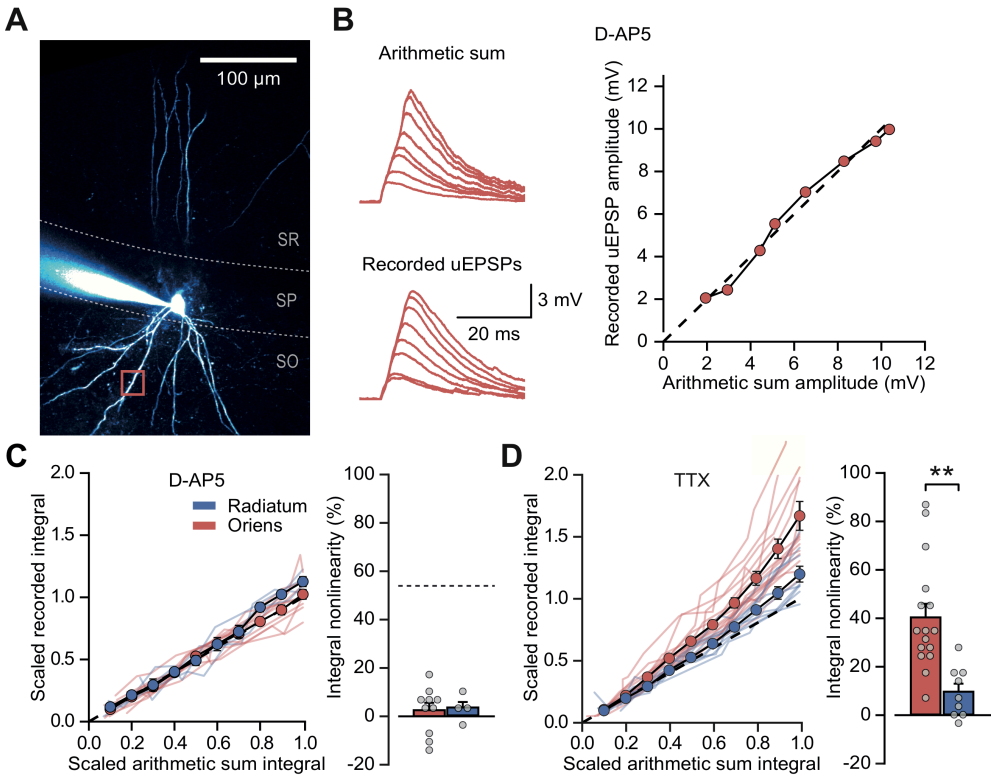

Figure 2: NMDARs mediate stratum oriens dendrite synaptic integration supralinearity: (**A**) Two-photon z-stack of PV+ interneuron in CA1 region of hippocampus. Red box marks glutamate uncaging location. (**B**) Comparison of arithmetic and recorded uEPSP summation waveforms in the presence of D-AP5. Right: peak recorded amplitude vs peak arithmetic amplitude. (**C**) Summary data of time-integrals plotted against arithmetic sum time-integrals for 14 dendritic locations recorded in D-AP5; n = 10 oriens, n = 4 radiatum. Right: quantified synaptic integration nonlinearity. The dashed line marks the average magnitude of oriens nonlinearity from **Fig. 1F**. (**D**) Summary data for 25 dendritic locations recorded in TTX; n = 16 oriens, n = 9 radiatum. Right: quantification of synaptic integration nonlinearity.

The dendrites of PV+ basket cells in stratum oriens are generally thinner and shorter than those in stratum radiatum[16]. This raises the possibility that oriens dendrites are depolarized more effectively by glutamate uncaging acting on AMPA receptors (AMPARs), because of a higher effective local input impedance, thereby enhancing relief of NMDARs from voltage-dependent block by Mg^{2+} [19]. To investigate the relationship between synaptic integration and dendritic geometry we used a detailed compartmental model of a CA1 PV+ interneuron (**Fig. 3A**). Voltage-dependent conductance densities and membrane properties were implemented according to previously published models[20,21], and the densities of synaptic AMPARs or NMDARs were initially assumed to be the same on oriens and radiatum dendrites. Simulations that closely followed the uncaging experiments, scanning across the range of experimentally measured locations, revealed supralinear summation of EPSPs recorded at the soma that was more pronounced for stratum oriens than for stratum radiatum dendrites (oriens vs radiatum time-integral nonlinearity: 42.5 ± 3.5 % vs 23.9 ± 2.3 *%, P* = 0.0005, **Fig. 3B**). This ~ 2-fold difference between strata was however smaller than the ~ 9-fold difference observed experimentally (oriens vs radiatum time-integral nonlinearity: 54.0 ± 10.1 % vs 6.3 ± 7.6 %; **Fig. 1**).

Feedback connections from local pyramidal cells onto CA1 PV+ interneurons have previously been reported to exhibit a higher NMDAR/AMPAR conductance ratio than Schaffer collateral feedforward synapses[11]. However, the low input resistance of PV+ interneurons, together with different dendritic morphologies in strata oriens and radiatum, confounds quantitative assessment of the relative density of NMDARs[22]. We minimized these pitfalls by recording postsynaptic excitatory currents (EPSCs) in a low (0.1 mM) extracellular Mg^{2+} solution (**Fig. 3C**) to partially relieve the Mg^{2+} block of NMDA receptors while holding PV+ interneurons at –60 mV. Pharmacological dissection of EPSCs revealed a >2-fold greater NMDAR/AMPAR charge ratio when stimulating in the alveus to excite axon collaterals of local pyramidal neurons[23], than when stimulating in stratum radiatum to excite Schaffer collaterals (charge ratio: 3.5 ± 0.7 vs 1.3 ± 0.3, *P* = 0.0017, n = 10, paired *t*-test; **Fig. 3C**). We further confirmed, using paired recordings, that action potentials evoked in CA1 pyramidal neurons elicited monosynaptic currents in PV+ interneurons with an NMDAR component (3 out of 5 connections tested; Fig. S8). Reducing the simulated NMDAR/AMPAR charge ratio at radiatum dendrites to half that of the oriens

dendrites improved agreement with the experimental data on dendritic integration nonlinearity (model data: 42.5 ± 3.5 % vs 8.5 ± 0.8 %; experimental data: 54.0 ± 10.1 % vs 6.3 ± 7.6 %; **Fig. 3D**). The striking difference in dendritic integration in oriens and radiatum dendrites can thus be explained by a combination of differential NMDAR expression and dendritic morphology.

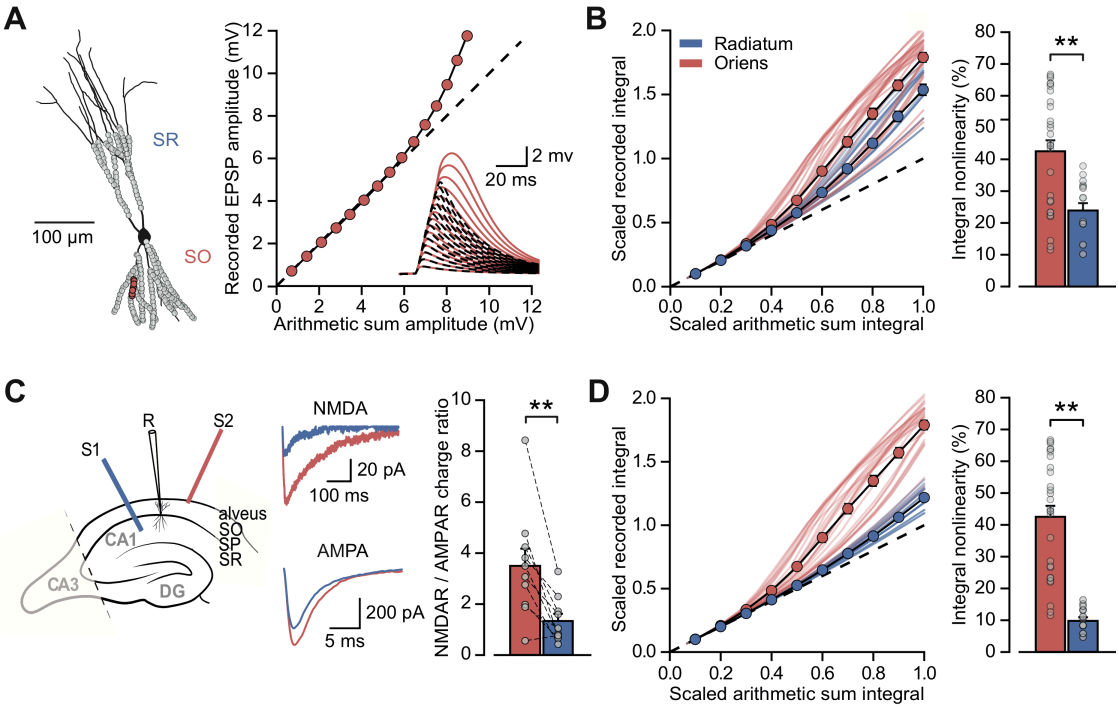

Figure 3: Differential NMDAR expression and dendrite morphology explain stratum-dependent synaptic integration difference. (**A**) Reconstruction of a PV+ interneuron (axon not shown). Simulated synaptic locations are shown in gray. Right: example simulated uncaging experiment at the synapses marked with red circles; graph shows recorded EPSP amplitudes vs arithmetic sum of EPSP ampltitues. Inset: red solid lines, recorded summation; dashed black lines, arithmetic summation; waveforms calculated from individual synaptic responses. (**B**) Scaled recorded time-integrals vs scaled arithmetic sum of time-integrals at all locations with equal NMDAR conductance. Right: quantified synaptic integration nonlinearity. n=16 radiatum, n=28 oriens. (**C**) Experimental setup for pharmacological dissection of NMDAR vs AMPAR conductance from feedforward and feedback inputs. Middle: example NMDAR and AMPAR traces from feedback (red) and feedforward (blue) inputs. Right: NMDAR:AMPAR charge ratios, respectively. n=10 (**D**) As **B**, but with reduced NMDAR:AMPAR ratio at radiatum dendrites.

Feedback recruitment of interneurons has been implicated in winner-takes-all mechanisms[24] and lateral inhibition, fundamental to a range of circuit computations such as sparsification of activity, pattern separation and place-code conversion[25,26]. To probe the computational implications of nonlinear integration of feedback inputs in stratum oriens dendrites of PV+ interneurons, we simulated the behavior of a network of spiking excitatory point neurons[27] receiving an asynchronous population-rate coded input, reciprocally connected to a single fast-spiking inhibitory neuron[28,29] (**Fig. 4A,B**). Excitatory neurons entered into a sparsely firing oscillatory state akin to a cortical gamma rhythm, with the simulated PV+ interneuron firing at around 40 Hz. The inhibitory neuron received simulated dual-component (AMPAR and NMDAR) synaptic conductances from the excitatory neuron layer, and nearby synapses were allowed to interact cooperatively and engage the non-ohmic behavior of NMDARs (Fig. S9). The strength of interaction between individual excitatory synapses on the interneuron fell off with distance in input space, consistent with experimental evidence for clustering of homotopic inputs on dendritic segments in principal neurons[30,31]. Excitatory neurons receiving a spatially compact 'hump' of excitation from the input layer cooperated in activating NMDARs on the interneuron to a greater extent than equivalent excitation dispersed randomly in input space (**Fig. 4B**). Recruitment of NMDAR conductances in the interneuron gradually sparsified principal cell firing over several oscillatory cycles, and thus maintained a sharp assembly representation (Fig. S10).

We then simulated interactions between two similar networks mutually inhibiting one another[2,3] to understand how NMDARs in the inhibitory neurons affect competition among cell assemblies. When one network received a stable and compact hump of excitation it was much more likely to be entrained than the competing network receiving an equal amount of spatially dispersed excitation. This difference disappeared when NMDARs were removed from the inhibitory neurons (**Fig. 4C**). Finally, we explored the ability of the combined network to 'lock' onto one of two competing but otherwise identical inputs presented to each sub-network. Because of simulated noise and neuronal accommodation, the combined network was able to 'flip' between the two inputs. The rate of flipping increased steeply when NMDARs were removed from the inhibitory neurons, leading it to flicker between the competing inputs, but was relatively unaffected by removing AMPARs (**Fig. 4D**).

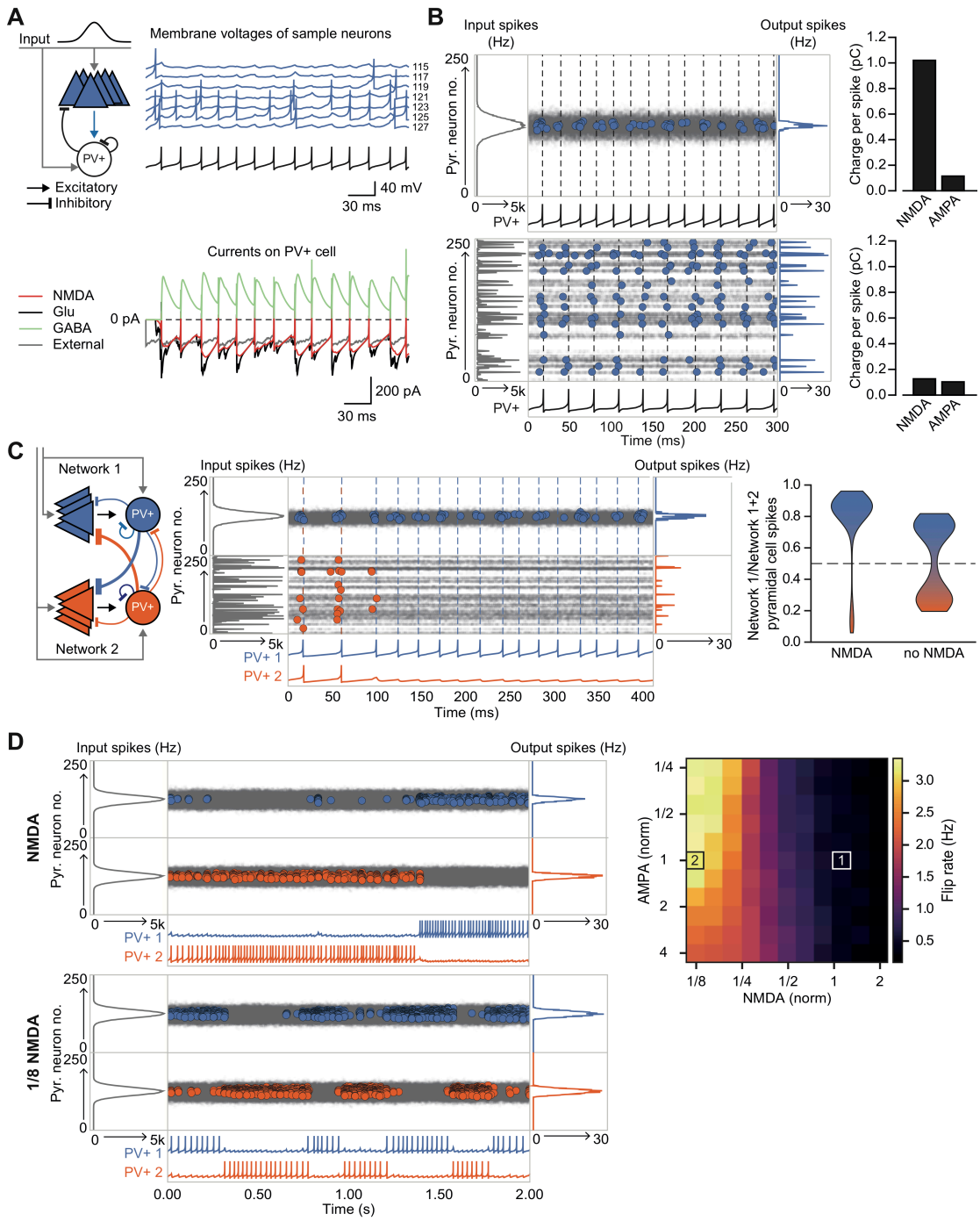

Figure 4: The role of NMDARs at feedback connections in cell assembly competition. (**A**) Top: schematic of network structure and voltage traces of interneuron (black) and principal cells (blue, cell # at right) during network simulation, and corresponding currents in interneuron (bottom). The network was driven by an asynchronous barrage of spikes, maximal in cell #125 ('clustered' input). (**B**) Summary plot of network simulation showing external input distribution (black), pyramidal cell firing (blue, circles), and interneuron firing (black, and vertical dashed lines), for clustered (top) and dispersed (bottom) external input. Right: average NMDAR and AMPAR charge in interneuron per principal neuron spike. (**C**) Lateral

inhibition between subnetworks driven by clustered or dispersed inputs. Middle: example simulation with NMDARs at feedback connections to interneuron. Right: summary of 250 simulations showing ratio of principal cell spikes for each subnetwork with and without NMDARs at feedback inputs onto interneuron. (**D**) Left: competing subnetworks with external input noise, with (top) and without (bottom) NMDARs. Right: plot of dominant network flip rate vs NMDAR and AMPAR conductance. White box labeled 1: baseline NMDAR simulation parameters; black box labeled 2: NMDARs down-scaled by 87.5%.

The present study shows that supralinear interactions among feedback, but not feedforward, excitatory inputs to PV+ interneurons is achieved by both differential expression of NMDARs and specialized dendritic properties. Dendritic NMDARs at feedback excitatory synapses allow a simulated network to lock onto a stable input represented by activity of spatially clustered synapses converging on part of the dendritic tree. We thus provide a simple mechanism for competition among neuronal assemblies represented by a sparsely firing population of excitatory neurons reciprocally coupled to inhibitory neurons. Extrapolating from the behavior of a spiking neural network model to information processing in the brain clearly depends on a number of assumptions, not least that the principles underlying NMDAR-dependent input integration observed in CA1 PV+ interneurons apply generally, and that clustering of homotopic inputs in dendritic segments obeys the same rules as in excitatory neurons[30,31]. Nevertheless, NMDAR-dependent supralinear integration in the feedback inhibitory loop potentially expands the computational power of a canonical cortical motif. It provides a mechanistic explanation for the finding that genetic ablation of NMDARs from PV+ interneurons degrades spatial representation in the hippocampus[9]. Destabilization of neuronal assemblies may also explain failure of sensory gating in schizophrenia[32], where impaired NMDAR-dependent excitation of PV+ interneurons has been implicated[33–35].

References and Notes

1. Buzsáki, G. Neural Syntax: Cell Assemblies, Synapsembles, and Readers. *Neuron* **68,** 362–385 (2010).
2. Trouche, S. *et al.* Recoding a cocaine-place memory engram to a neutral engram in the hippocampus. *Nat. Neurosci.* **19,** 564–567 (2016).
3. Geisler, C., Robbe, D., Zugaro, M., Sirota, A. & Buzsáki, G. Hippocampal place cell assemblies are speed-controlled oscillators. *Proc. Natl. Acad. Sci.* **104,** 8149–8154 (2007).
4. Kim, H., Ährlund-Richter, S., Wang, X., Deisseroth, K. & Carlén, M. Prefrontal Parvalbumin Neurons in Control of Attention. *Cell* **164,** 208–218 (2016).
5. Jonas, P., Bischofberger, J., Fricker, D. & Miles, R. Interneuron Diversity series: Fast in, fast out – temporal and spatial signal processing in hippocampal interneurons. *Trends Neurosci.* **27,** 30–40 (2004).
6. Pouille, F. & Scanziani, M. Enforcement of temporal fidelity in pyramidal cells by somatic feed-forward inhibition. *Science* **293,** 1159–63 (2001).
7. Pouille, F., Marin-Burgin, A., Adesnik, H., Atallah, B. V & Scanziani, M. Input normalization by global feedforward inhibition expands cortical dynamic range. *Nat. Neurosci.* **12,** 1577–1585 (2009).
8. Carlén, M. *et al.* A critical role for NMDA receptors in parvalbumin interneurons for gamma rhythm induction and behavior. *Mol. Psychiatry* **17,** 537–548 (2012).
9. Korotkova, T., Fuchs, E. C., Ponomarenko, A., von Engelhardt, J. & Monyer, H. NMDA Receptor Ablation on Parvalbumin-Positive Interneurons Impairs Hippocampal Synchrony, Spatial Representations, and Working Memory. *Neuron* **68,** 557–569 (2010).
10. Jadi, M. P., Behrens, M. M. & Sejnowski, T. J. Abnormal Gamma Oscillations in N-Methyl-D-Aspartate Receptor Hypofunction Models of Schizophrenia. *Biol. Psychiatry* **79,** 716–726 (2016).
11. Le Roux, N., Cabezas, C., Böhm, U. L. & Poncer, J. C. Input-specific learning rules at excitatory synapses onto hippocampal parvalbumin-expressing interneurons. *J. Physiol.* **591,** 1809–22 (2013).
12. Stuart, G. J. & Spruston, N. Dendritic integration: 60 years of progress. *Nat.*

Neurosci. **18,** 1713–1721 (2015).

13. Poirazi, P. & Mel, B. W. Impact of active dendrites and structural plasticity on the memory capacity of neural tissue. *Neuron* **29,** 779–796 (2001).
14. Losonczy, A. & Magee, J. C. Integrative properties of radial oblique dendrites in hippocampal CA1 pyramidal neurons. *Neuron* **50,** 291–307 (2006).
15. Gasparini, S. State-Dependent Dendritic Computation in Hippocampal CA1 Pyramidal Neurons. *J. Neurosci.* **26,** 2088–2100 (2006).
16. Gulyás, A. I., Megías, M., Emri, Z. & Freund, T. F. Total number and ratio of excitatory and inhibitory synapses converging onto single interneurons of different types in the CA1 area of the rat hippocampus. *J. Neurosci.* **19,** 10082–10097 (1999).
17. Hu, H., Martina, M. & Jonas, P. Dendritic mechanisms underlying rapid synaptic activation of fast-spiking hippocampal interneurons. *Science (80-.).* **327,** 52–58 (2010).
18. Chiovini, B. *et al.* Dendritic Spikes Induce Ripples in Parvalbumin Interneurons during Hippocampal Sharp Waves. *Neuron* **82,** 908–924 (2014).
19. Branco, T., Clark, B. A. & Häusser, M. Dendritic discrimination of temporal input sequences in cortical neurons. *Science (80-.).* **329,** 1671–1675 (2010).
20. Nörenberg, A., Hu, H., Vida, I., Bartos, M. & Jonas, P. Distinct nonuniform cable properties optimize rapid and efficient activation of fast-spiking GABAergic interneurons. *Proc. Natl. Acad. Sci. U. S. A.* **107,** 894–9 (2010).
21. Hu, H. & Jonas, P. A supercritical density of Na(+) channels ensures fast signaling in GABAergic interneuron axons. *Nat. Neurosci.* **17,** 686–693 (2014).
22. Williams, S. R. & Mitchell, S. J. Direct measurement of somatic voltage clamp errors in central neurons. *Nat. Neurosci.* **11,** 790–798 (2008).
23. Pouille, F. & Scanziani, M. Routing of spike series by dynamic circuits in the hippocampus. *Nature* **429,** 717–723 (2004).
24. de Almeida, L., Idiart, M. & Lisman, J. E. A second function of gamma frequency oscillations: an E%-max winner-take-all mechanism selects which cells fire. *J. Neurosci. Off. J. Soc. Neurosci.* **29,** 7497–7503 (2009).
25. Hu, H., Gan, J. & Jonas, P. Interneurons. Fast-spiking, parvalbumin^{+} GABAergic interneurons: from cellular design to microcircuit function. *Science (80-.).* **345,** 1255263 (2014).

26. Roux, L. & Buzsáki, G. Tasks for inhibitory interneurons in intact brain circuits. *Neuropharmacology* **88,** 10–23 (2015).
27. Izhikevich, E. M. Simple model of spiking neurons. *IEEE Trans. Neural Networks* **14,** 1569–1572 (2003).
28. Ferguson, K. A., Huh, C. Y. L., Amilhon, B., Williams, S. & Skinner, F. K. Simple, biologically-constrained CA1 pyramidal cell models using an intact, whole hippocampus context. *F1000Research* **3,** 104 (2014).
29. Ferguson, K. A., Huh, C. Y. L., Amilhon, B., Williams, S. & Skinner, F. K. Experimentally constrained CA1 fast-firing parvalbumin-positive interneuron network models exhibit sharp transitions into coherent high frequency rhythms. *Front. Comput. Neurosci.* **7,** 144 (2013).
30. Wilson, D. E., Whitney, D. E., Scholl, B. & Fitzpatrick, D. Orientation selectivity and the functional clustering of synaptic inputs in primary visual cortex. *Nat. Neurosci.* **19,** 1003–9 (2016).
31. Iacaruso, M. F., Gasler, I. T. & Hofer, S. B. Synaptic organization of visual space in primary visual cortex. *Nature* **547,** 449–452 (2017).
32. Javitt, D. C. & Freedman, R. Sensory processing dysfunction in the personal experience and neuronal machinery of schizophrenia. *Am. J. Psychiatry* **172,** 17–31 (2015).
33. Lisman, J. E. *et al.* Circuit-based framework for understanding neurotransmitter and risk gene interactions in schizophrenia. *Trends Neurosci.* **31,** 234–242 (2008).
34. Nakazawa, K. *et al.* GABAergic interneuron origin of schizophrenia pathophysiology. *Neuropharmacology* **62,** 1574–1583 (2012).
35. Bygrave, A. M. *et al.* Knockout of NMDA-receptors from parvalbumin interneurons sensitizes to schizophrenia-related deficits induced by MK-801. *Transl. Psychiatry* **6,** e778 (2016).

Acknowledgements:

We are grateful to members of the Experimental Epilepsy Group at the UCL Institute of Neurology, Peter Latham and Arnd Roth for advice and technical assistance. This work was supported by the Wellcome Trust and the Brain Research Trust.